

IDWA Number B50011/Member Contract No. ZA0226  
Report CRAD-9408-TR-3027

4.2.6  
DTF 26-02-03

# High Speed Research - Airframe Technology

## Airframe Materials & Structures 4.2.6 - Aeroelasticity

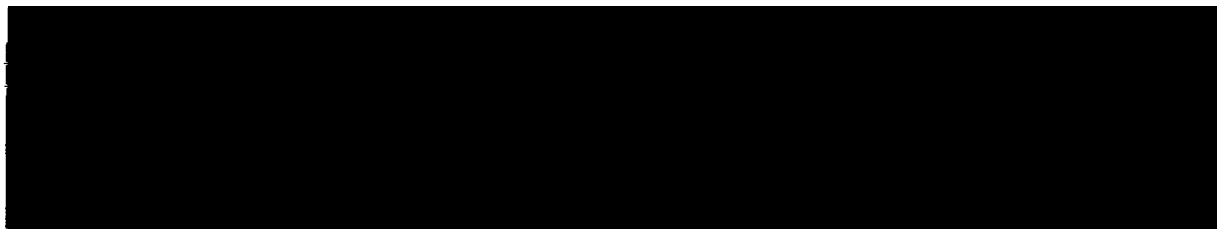


### Technical Milestone Report:

### Preliminary Evaluation of Nonlinear Effects on TCA Flutter

Report Date: February 20, 1998

Prepared for  
The Boeing Company  
Seattle, Washington 98124-2207



#### LIMITATION CHANGE

This document was formally controlled by Limited  
Exclusive Rights under NASA Contract NAS1-20220  
and has been decontrolled per authority of NASA LaRC  
and The Boeing Company. (HSR Integrated Planning  
Team Minutes dated 5/27/99)  
Changed by CXH Date 10/4/99

**SIGNATURES**

**MDC HSR II Airframe Task 26 (WBS 4.2.6)  
Aeroelasticity  
Preliminary Evaluation of Nonlinear Effects on TCA Flutter  
IDWA Number B50011/Member Contract No. ZA0226**

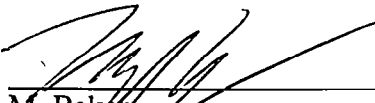
**MDC Report CRAD-9408-TR-3027**

**Report Date: 2/20/98**

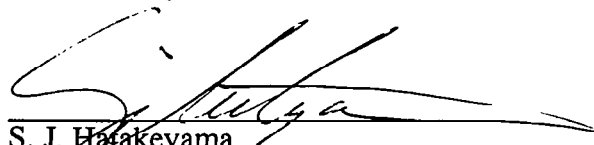
Report prepared by:

  
A. Arslan  
High Speed Aerodynamics

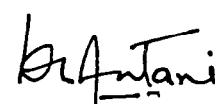
Report approved by:

  
M. Baker  
Task Manager  
Aeroelasticity

Report approved by:

  
S. J. Hatakeyama  
Program Manager  
Airframe Materials & Structures

Report approved by:

  
T. Antani  
Senior Manager  
Design & Technology

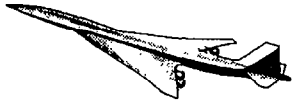
## **FOREWORD**

This document consists of a set of presentation charts and accompanying facing-page text, and is being submitted to satisfy the deliverable "Preliminary Evaluation of Nonlinear Effects on TCA Flutter" (WBS 4.2.6.3) of the High Speed Research II - Airframe Technologies Contract NAS1-20220.

The work reported here is part of the effort in Aeroelasticity, and was performed by a team of experts from Boeing Long Beach. The NASA technical point of contact for this task is Rob Scott of NASA Langley Research Center.

The key personnel responsible for this effort were:

<b>Name</b>	<b>Function</b>
Mr. Alan Arslan	High Speed Aerodynamics
Dr. Peter Hartwich	High Speed Aerodynamics
Dr. Myles Baker	Sub-Task PI, Aeroelasticity



*High Speed Aerodynamics, Long Beach*

# **Non-Linear TCA Flutter Studies**

Alan E. Arslan, Peter M. Hartwich, and Myles L. Baker

The Boeing Company  
Long Beach, California

NASA/Industry HSR Airframe Review  
Los Angeles, California  
February 9-13, 1998

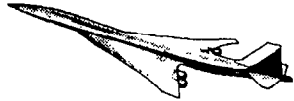


# Non-Linear TCA Flutter Studies

The objective of this study is to investigate the effect of nonlinear aerodynamics, especially at high angles-of-attack with leading-edge separation, on the TCA flutter properties at transonic speeds. In order to achieve that objective, flutter simulations with Navier-Stokes CFD must be performed.

To this end, time-marching Navier-Stokes solutions are computed for the TCA wing/body configuration at high angles-of-attack in transonic flight regimes. The approach is to perform non-linear flutter calculations on the TCA at two angles-of-attack, the first one being a case with attached flow ( $\alpha=2.8^\circ$ ) and the second one being a high angle-of-attack case with a wing leading-edge vortex ( $\alpha=12.11^\circ$ ). Comparisons of the resulting histories and frequency damping information for both angles-of-attack will evaluate the impact of high-alpha aerodynamics on flutter.

# Non-Linear TCA Flutter Studies



*High Speed Aerodynamics, Long Beach*

- **Objective:** Study the effect of nonlinear aerodynamics due to LE separation on the TCA flutter properties at transonic speeds
- **Approach:**
  - Perform nonlinear flutter calculations on the TCA at two flight conditions (MT-3 mass case at Mach 1.2 at  $V_D$ ):
    - Low  $\alpha$  ( $\alpha=2.8^\circ$ , without LE vortices)
    - High  $\alpha$  ( $\alpha=12.1^\circ$ , with LE vortices)
  - Compare resulting histories for structural responses & frequency damping information to assess impact of high-alpha on flutter

# CFD Approach

Due to schedule constraints, it was decided to use an existing grid for the rigid TCA wing/body configuration for which asymptotic steady-state solutions at a Reynolds number of 40 million already existed for the two angles-of-attack considered in the present study. The ACE (Aeroelastic Concept Engineering) loads activity provided the starting point for this study which consisted of the TCA wing/body with the outboard leading-edge flap deflected by  $8^\circ$ .

The grid was of C-O topology with 93x281x69 nodes with spanwise clustering for the flap segments (leading and trailing-edge). The FlexMesh grid perturbation package was used to perturb the grid for the aeroelastic deflections. Modifications to FLEXMESH are required to get acceptable perturbed grid quality for the large aeroelastic deflections and fine grids required for the N-S solutions.

The Navier-Stokes analyses were conducted with the CFL3D.AE-BA code with the Baldwin-Lomax turbulence model. The Degani-Schiff option was turned on to improve the accuracy of the solutions at angles-of-attack where wing leading-edge vortices are expected to occur. The time-accurate approach was also used. The flow conditions were  $M_\infty = 1.2$  at  $V_D$  ( $q = 758$  psf),  $Re_c = 40 \times 10^6$ ,  $\alpha = 2.83^\circ, 12.11^\circ$ . For this freestream Mach number, rapid convergence of the solutions to steady or to precise states was experienced. Thus, to ensure rapid turnaround  $M_\infty = 1.2$  was chosen for the freestream Mach number. The structural equations (dynamic system equations) are linear and used 22 mode shapes, corresponding to the MT-3 mass case (max TOGW, forward C.G., lumped payload).

# CFD Approach



*High Speed Aerodynamics, Long Beach*

- Configuration:
  - TCA W/B/LE flap (ACE Loads studies)
- Grid Generation:
  - Preprocess for flaps / flap deflection
  - FlexMesh for grid perturbation
- Analysis:
  - CFL3D.AE-BA, N-S, Badwin-Lomax (with Degani-Schiff modification), time-accurate approach
  - $M_\infty = 1.2$ ,  $Re_c = 40$  million,  $\alpha = 2.83^\circ, 12.11^\circ$
  - Linear structural equations, 22 mode shapes,  $q_\infty = 758.3$  psi





# Simulation Procedure

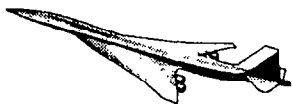
The simulation procedure consists of three steps.

The first step is to obtain a converged solution on a rigid configuration. This was obtained from the ACE loads activity.

As a second step, a static aeroelastic solution is computed. Here, the use of structural damping ( $\zeta = 0.99$ ) promotes a faster convergence of the static aeroelastic solution. The ACE loads runs suggested the use of 0.94 ms for the time-accurate approach (about 1000 iterations to go back and forth from the grid leading-edge to exit planes). This value corresponds to a non-dimensional time step size of 11.25. Since the time step to compute the highest frequency cycle in 40 iterations had a non-dimensional value of 28, the use of a larger time step of about 18 was acceptable.

The last step consists of the actual flutter simulation. The simulation is started with an initial perturbation or “ping” applied to the generalized velocity of every vibration mode. The magnitude of the perturbation was chosen to be 10% of the amplitude of the static generalized deflections. Approximately three periods of the dominant frequency were simulated, which was sufficient to get converged frequency and damping estimates.

# Simulation Procedure



*High Speed Aerodynamics, Long Beach*

- **Step1:** Obtain converged solution on rigid configuration (overlap with ACE Loads activity)
- **Step2:** Static aeroelastic coupling
  - Structural damping for faster convergence
  - Non-dimensional time step of 0.94/1.52 ms for the two respective angles-of-attack
- **Step3:** Flutter simulation
  - Initial perturbation (~10%) of generalized displacement velocities
  - About 3 periods of the dominant frequency

# Convergence History for the TCA W/B/LE Flap

The chart below shows the convergence history for the static run at  $\alpha = 2.83^\circ$ . Initially the rigid solution was run for loads applications. Therefore the convergence criteria used were different from the criteria for cruise point simulations and consisted of monitoring the sectional lift and center of pressure instead of residuals and drag convergence. The coarse and medium meshes were run in the steady-flow mode and the time-accurate advance was turned on for the fine mesh with three sub-iterations. Afterwards, the aeroelastic coupling was turned on with near-critical structural damping, and the static aeroelastic solution was computed in approximately 500 additional cycles.

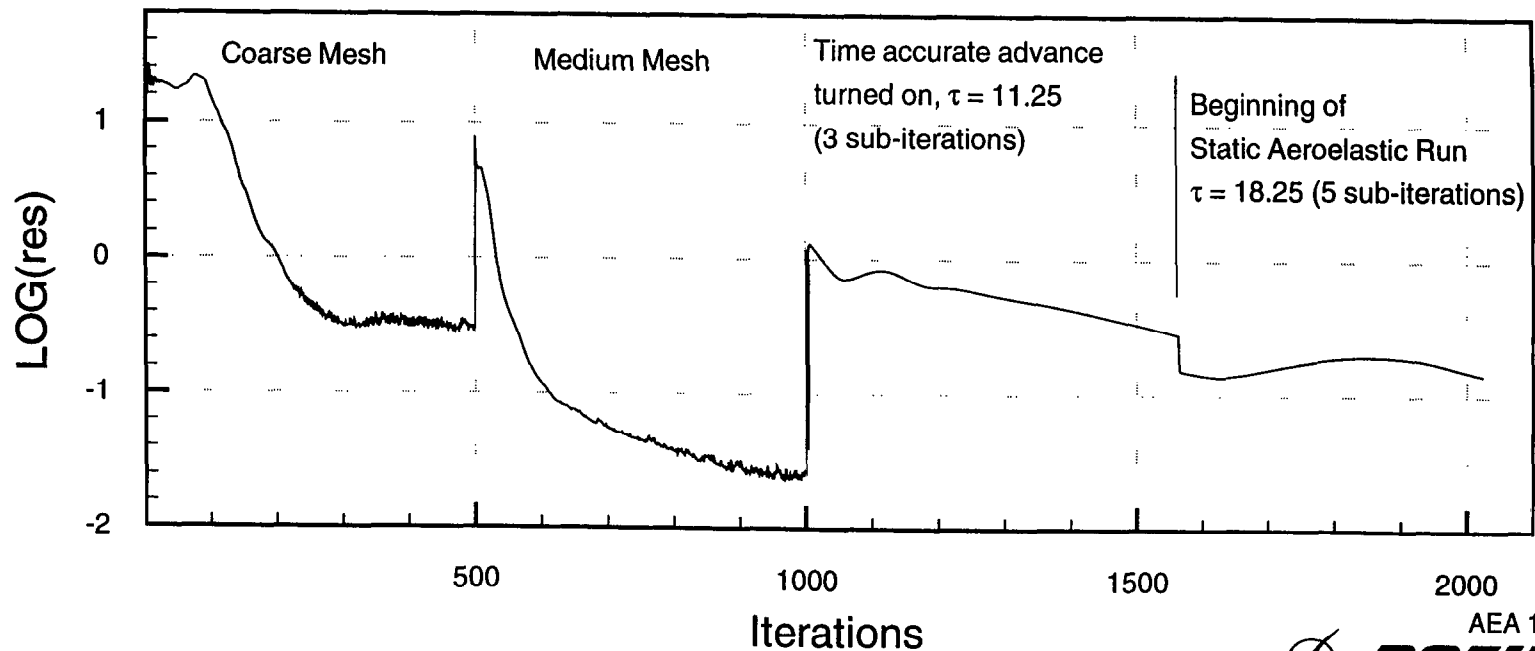
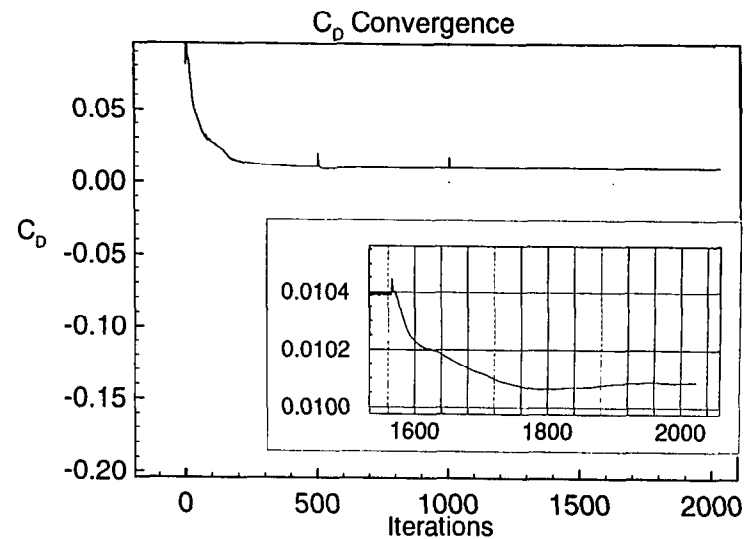
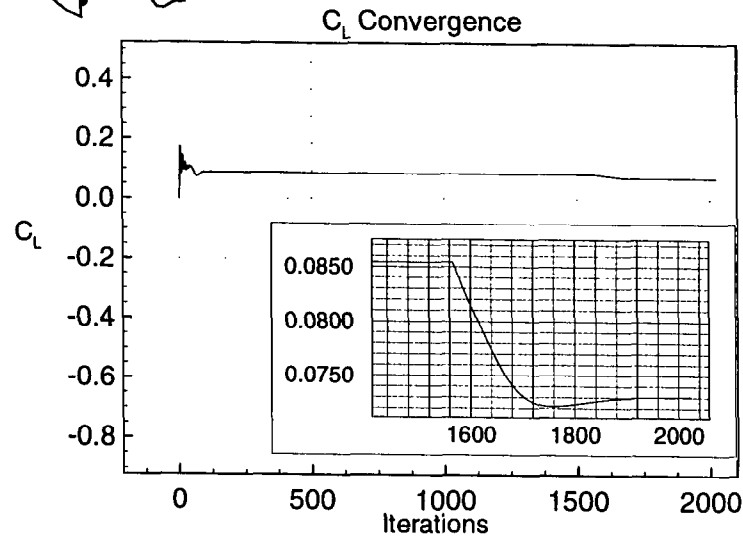


# Convergence History for the TCA W/B/LE Flap Aeroelastic Configuration

CFL3D N-S Baldwin-Lomax Degani-Schiff,  $Re_c=40 \times 10^6$ ;  $M=1.20$ ;  $\alpha=2.83^\circ$ ; C-O(93x281x69)



High Speed Aerodynamics, Long Beach



AEA 12/19/97



# Time History of Generalized Displacements

The chart below shows the time histories of the generalized displacements for the TCA configuration at  $\alpha = 2.83^\circ$ . The four modes with the largest generalized displacements are plotted. The curves associated with the four modes are almost flat for the last 0.1 sec indicating adequate convergence of the structural deflections. These solutions are used as starting solutions for flutter computations. We only compute static aeroelastic solutions for reasons of maximum efficiency. This approach reduces the transients in a flutter calculation.



# Time History of Generalized Displacements for TCA W/B/LE Flap Aeroelastic Configuration, Static Case

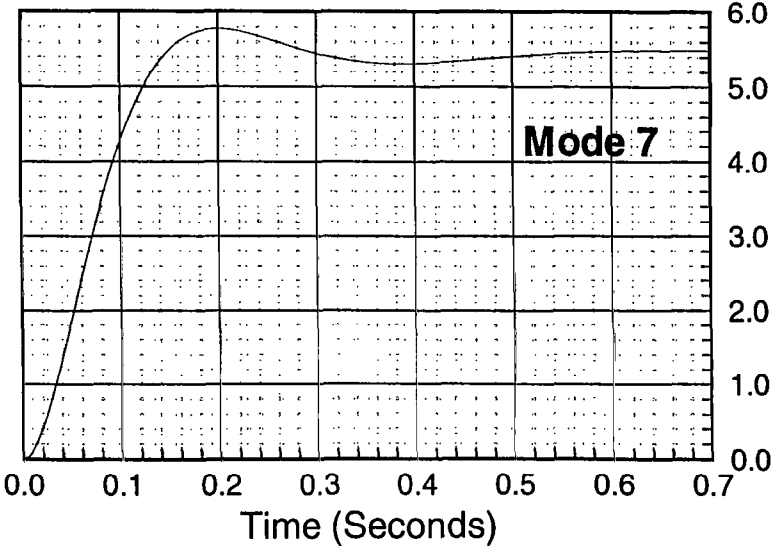
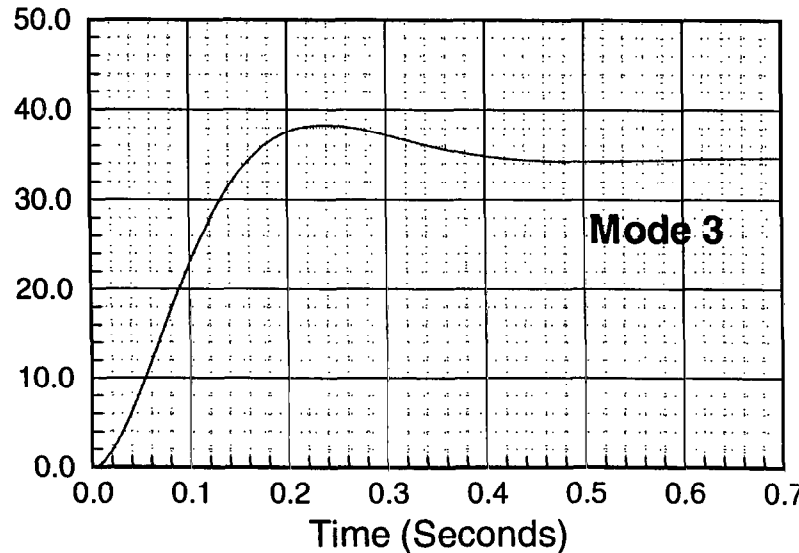
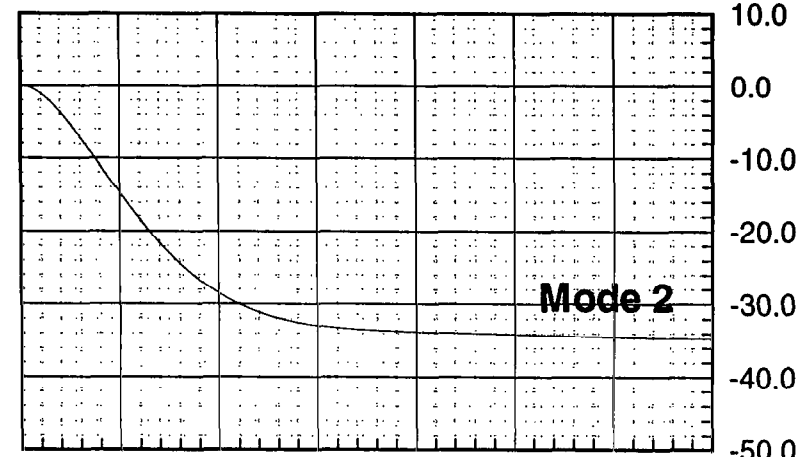
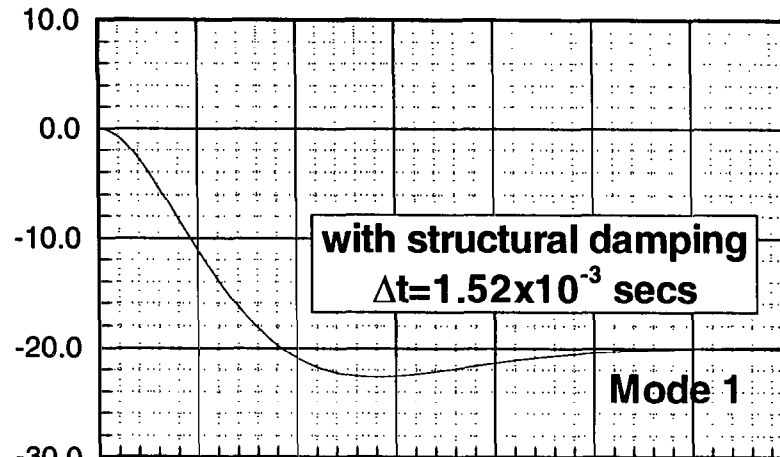


High Speed Aerodynamics, Long Beach

CFL3D.AE-BA, N-S, Baldwin-Lomax (D-S),  $M_\infty=1.2$ ,  $\alpha=2.83^\circ$ ,  $q_\infty=758.3$  psf  
(93x281x69 C-O Grid)

Generalized  
Displacement

Generalized  
Displacement



# Flow Analysis of the TCA Wing/Body/LE Flap

The chart below shows a comparison of the flowfields for both rigid and aeroelastic configurations at  $\alpha = 2.83^\circ$  for the TCA wing/body with the outboard leading-edge flap deflected by  $8^\circ$ . The right wing of each configuration shows normalized cross-sectional total pressure cuts. The left wing shows surface  $C_p$  distributions and streamlines. As expected, both configurations show attached flowfields. Suction along the outboard LE flap edge is observed for both configurations (color transition from red to green). For this low- $\alpha$  case, the wing loading was relatively low, and the resulting structural deflections are relatively small, so large changes in the flowfield due to aeroelastic effects are not evident.

# Flow Analysis of the TCA Wing/Body/LE Flap



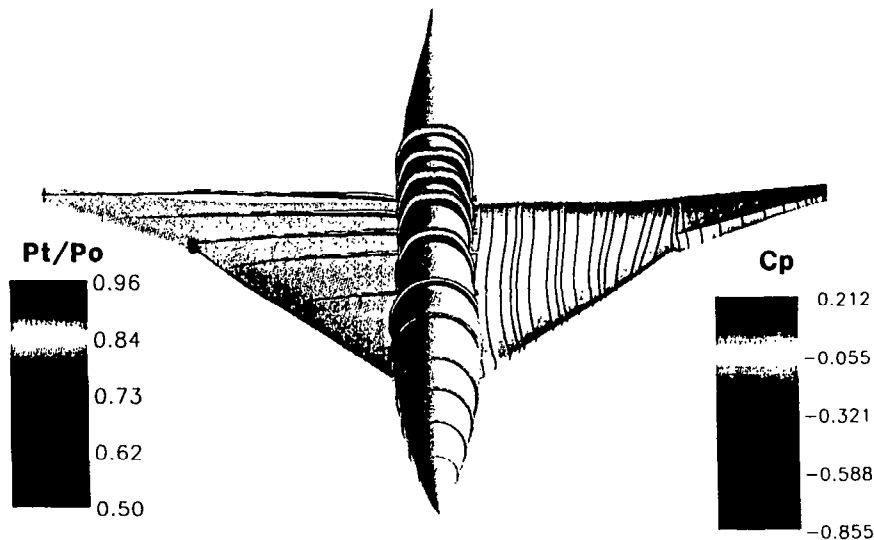
High Speed Aerodynamics, Long Beach

Configuration with and without Aeroelastic Deflections

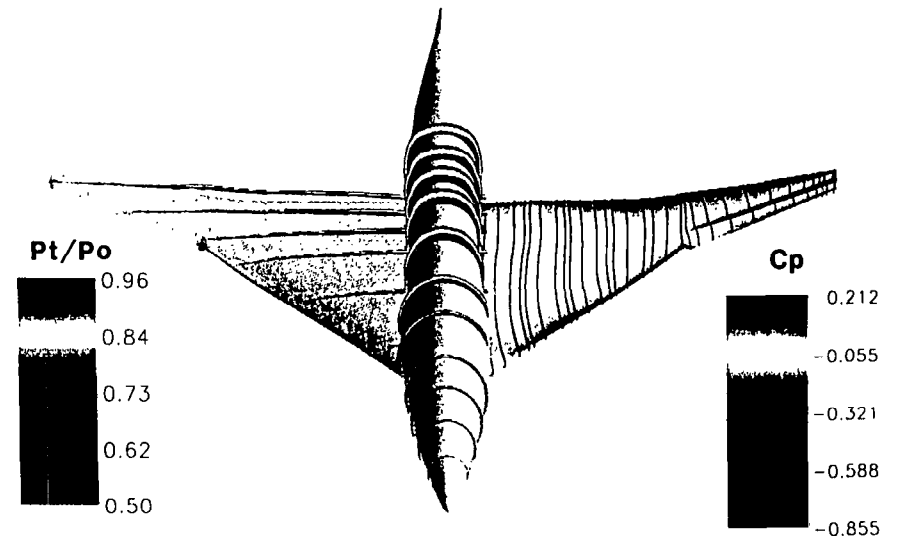
Cross-Sectional Total Pressure Cuts, Surface Cp Distributions and Streamlines

CFL3D, N-S, Baldwin-Lomax D-S,  $M_\infty = 1.2$ ,  $\alpha = 2.83^\circ$ ,  $Re_C = 40$  million

(C-O Grid 93x281x69)



Rigid Configuration



Aeroelastic Configuration

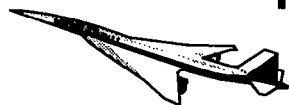


# Pressure Distributions for the TCA W/B/LE Flap

The three figures below show the pressure cuts for the two solutions shown in the previous chart. No significant differences are observed before the 53.9% span station. At the two outboard stations, the unloading can be clearly seen from the pressure curves. The airfoil cuts indicate a decrease in twist of the airfoil sections. Also, the suction around the leading edge is significantly reduced due to the leading-edge flap deflection. However, for the 85% station the suction around the leading-edge has increased for the aeroelastic configuration. This increase in suction is due to the aeroelastic washout.



# Pressure Distributions for the TCA W/B/LE Flap Rigid vs. Aeroelastic Configuration, Static Case



High Speed Aerodynamics, Long Beach

CFL3D.AE-BA, N-S, Baldwin-Lomax (D-S),  $M_\infty = 1.2$ ,  $\alpha = 2.83^\circ$ ,  $Re_c = 40$  million,  $q_\infty = 758.3$  psf

Span Station

85.0 %

68.0 %

53.9 %

41.3 %

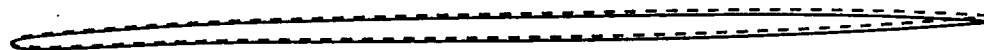
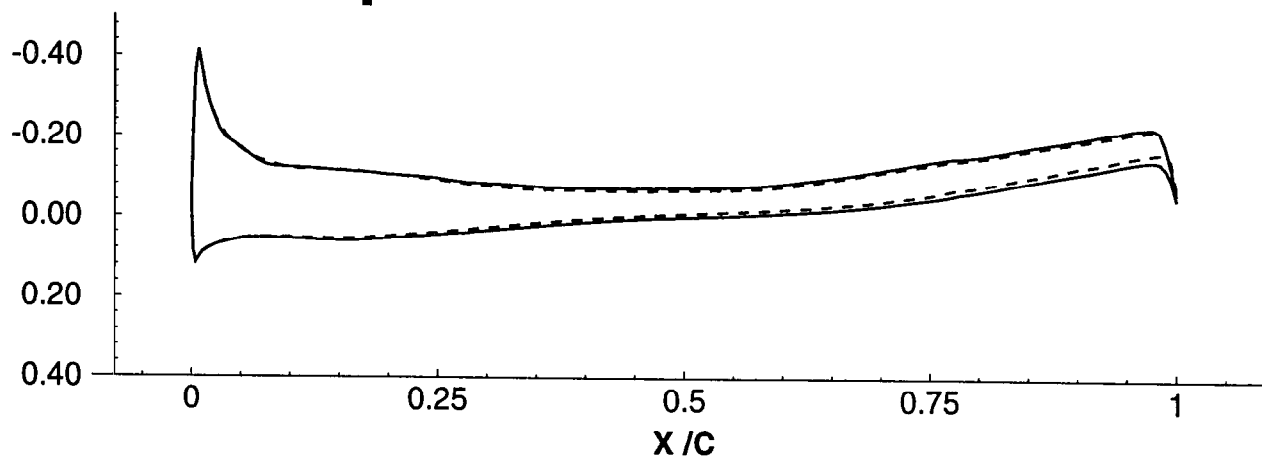
32.6 %

19.9 %

— Rigid  
- - Aeroelastic

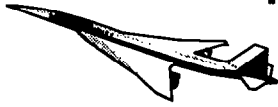
$C_p$

Span Station = 53.9%



**BOEING**

# Pressure Distributions for the TCA W/B/LE Flap Rigid vs. Aeroelastic Configuration, Static Case



High Speed Aerodynamics, Long Beach

CFL3D.AE-BA, N-S, Baldwin-Lomax (D-S),  $M_\infty = 1.2$ ,  $\alpha = 2.83^\circ$ ,  $Re_c = 40$  million,  $q_\infty = 758.3$  psf

Span Station

85.0 %

68.0 %

53.9 %

41.3 %

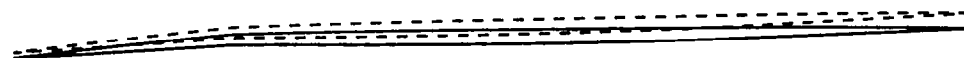
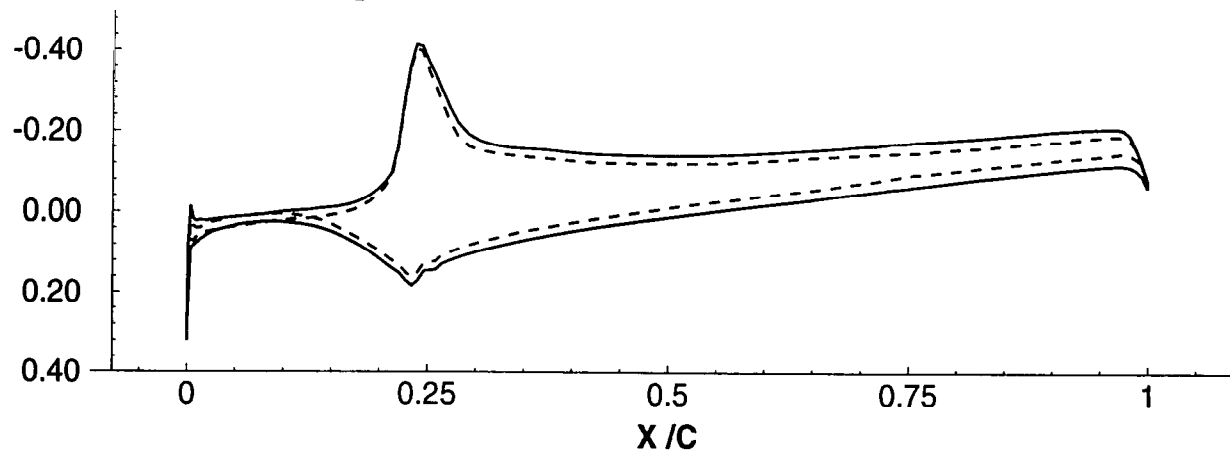
32.6 %

19.9 %

— Rigid  
- - Aeroelastic

$C_p$

Span Station = 68.0%



# Pressure Distributions for the TCA W/B/LE Flap Rigid vs. Aeroelastic Configuration, Static Case



High Speed Aerodynamics, Long Beach

CFL3D.AE-BA, N-S, Baldwin-Lomax (D-S),  $M_\infty = 1.2$ ,  $\alpha = 2.83^\circ$ ,  $Re_c = 40$  million,  $q_\infty = 758.3$  psf

Span Station

85.0 %

68.0 %

53.9 %

41.3 %

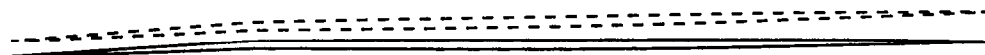
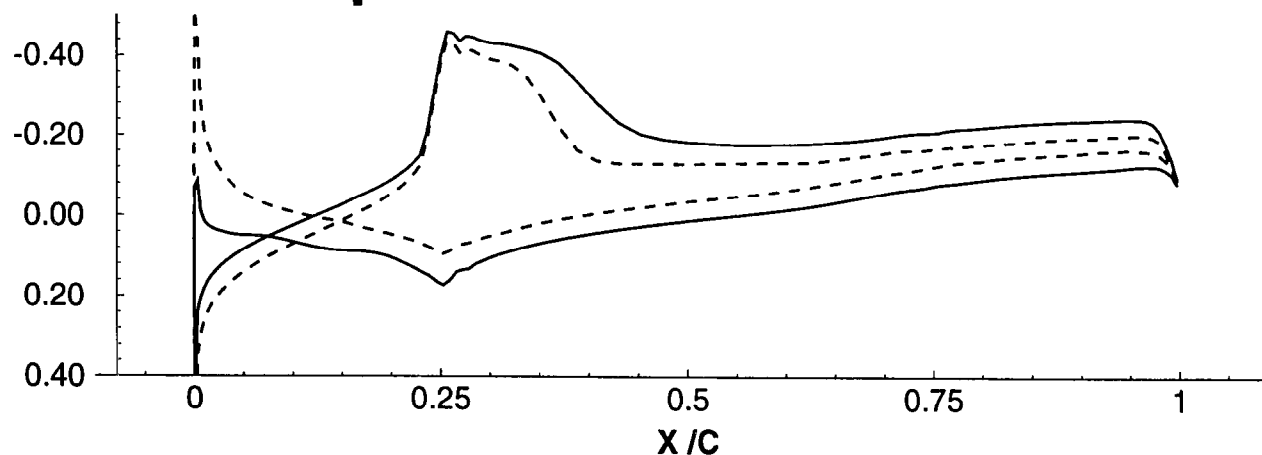
32.6 %

19.9 %

— Rigid  
- - Aeroelastic

$C_p$

Span Station = 85.0%



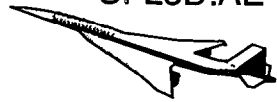
# Convergence History for the TCA W/B/LE Flap Aeroelastic Configuration

The chart below shows the convergence history for the static run at  $\alpha = 12.11^\circ$ . The rigid case is run in the steady-flow mode and a two order of magnitude reduction of the residual was observed for all three grid levels. The time-accurate aeroelastic simulation was started at 1500 iterations. Approximately 1200 iterations were required for convergence of the aeroelastic case (compared to the 500 iterations required for the low- $\alpha$  condition).



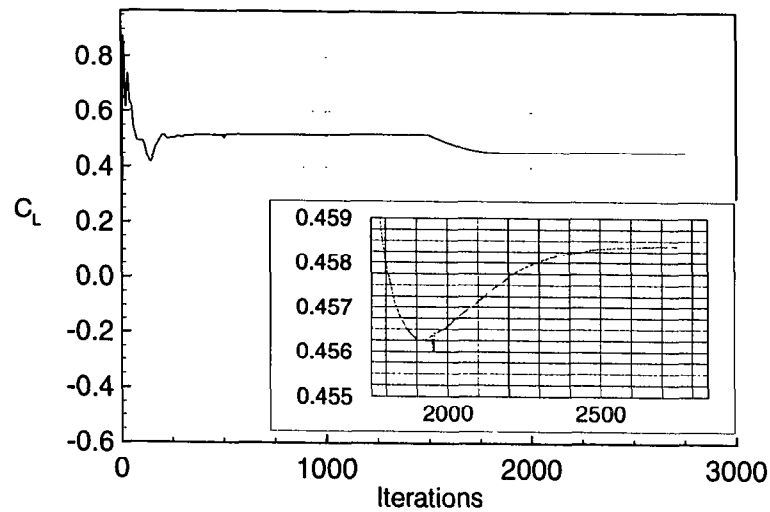
# Convergence History for the TCA W/B/LE Flap Aeroelastic Configuration

CFL3D.AE-BA, N-S, Baldwin-Lomax Degani-Schiff;  $Re_c=40 \times 10^6$ ;  $M_\infty=1.20$ ;  $\alpha=12.11^\circ$ ; C-O(93x281x69)

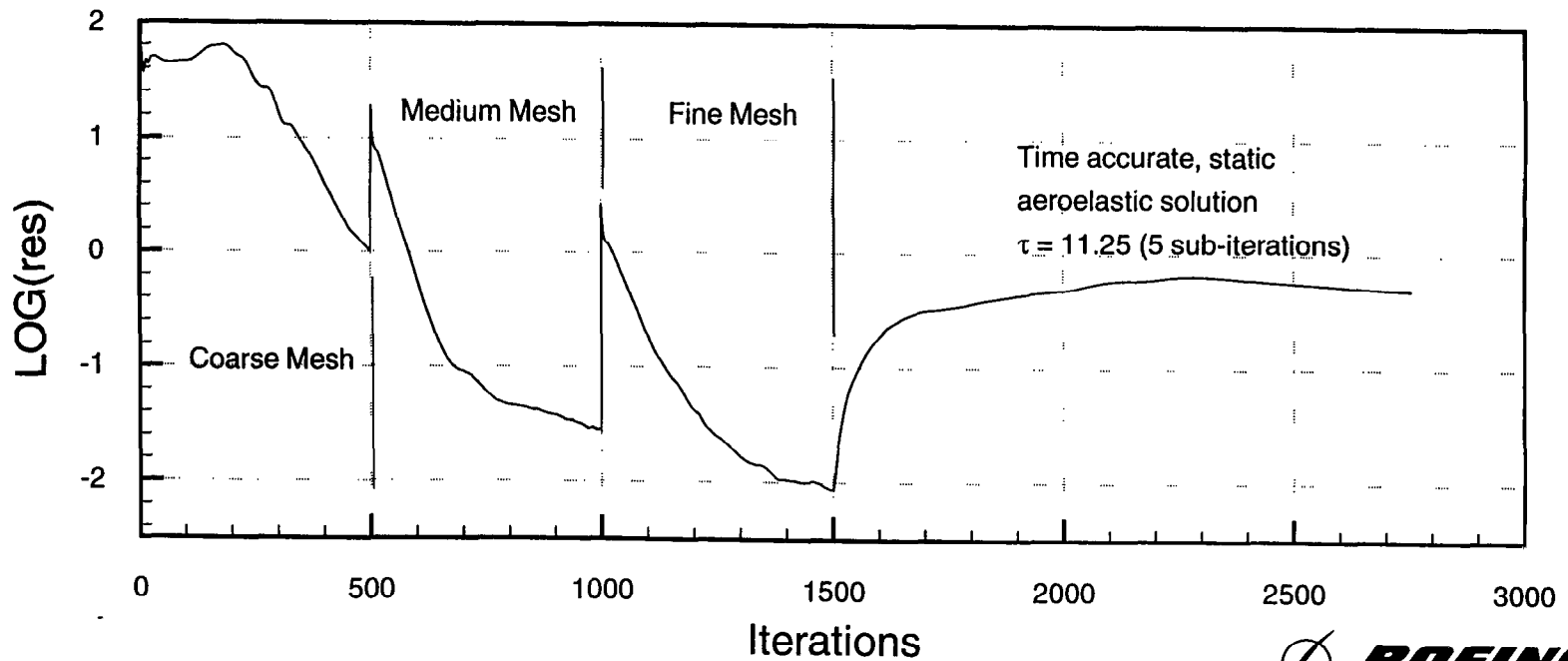
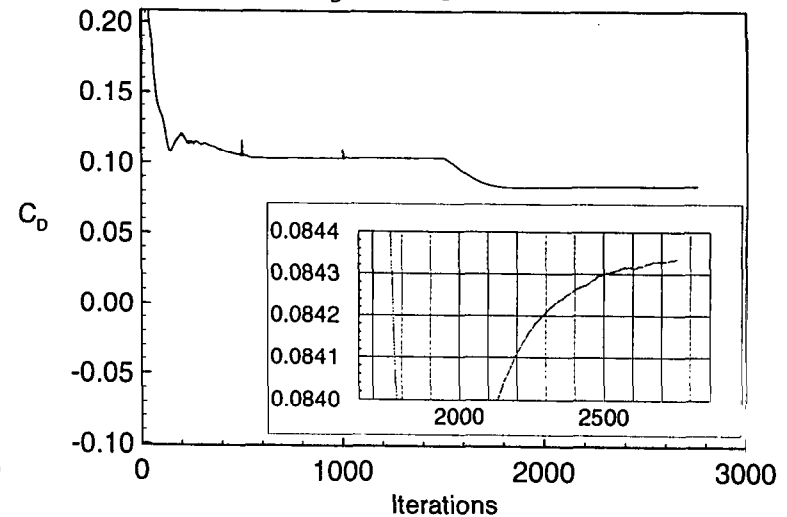


High Speed Aerodynamics, Long Beach

$C_L$  Convergence



$C_D$  Convergence



# Time History of the Generalized Displacements

The chart below shows the time histories of the generalized displacements for the TCA configuration at  $\alpha = 12.11^\circ$ . Again, the four modes with the largest displacements are plotted. The curves associated with the four modes are almost flat for the last 0.3 sec indicating adequate convergence of the structural deflections. For modes 1, 2, and 3, the magnitude of the generalized displacements is about 6 times that of the lower angle-of-attack case. This is an expected angle-of-attack (increase in lift) effect. The opposite trend is observed for mode 7.





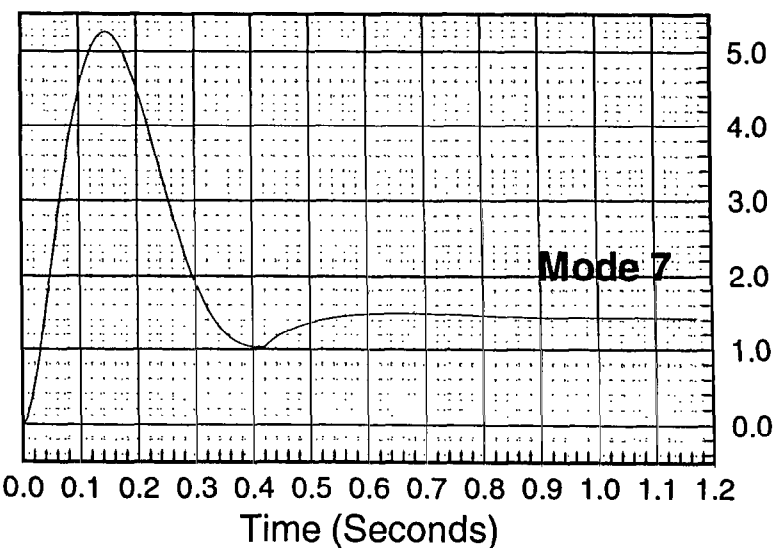
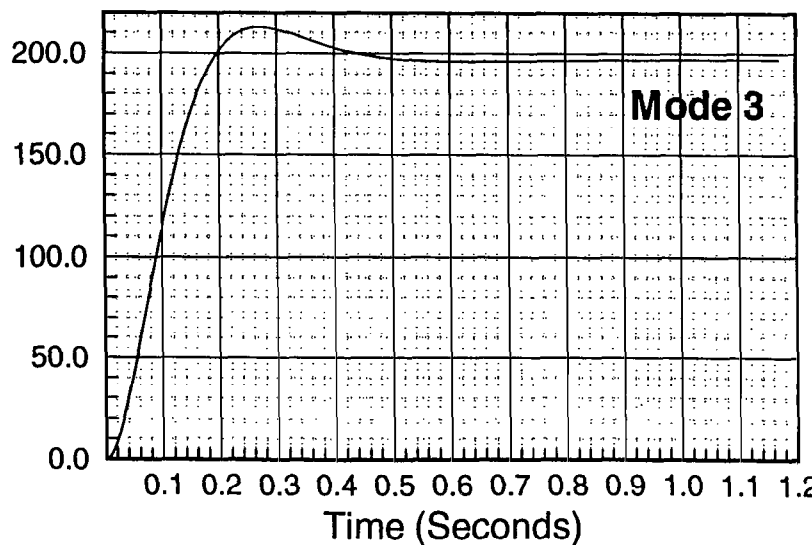
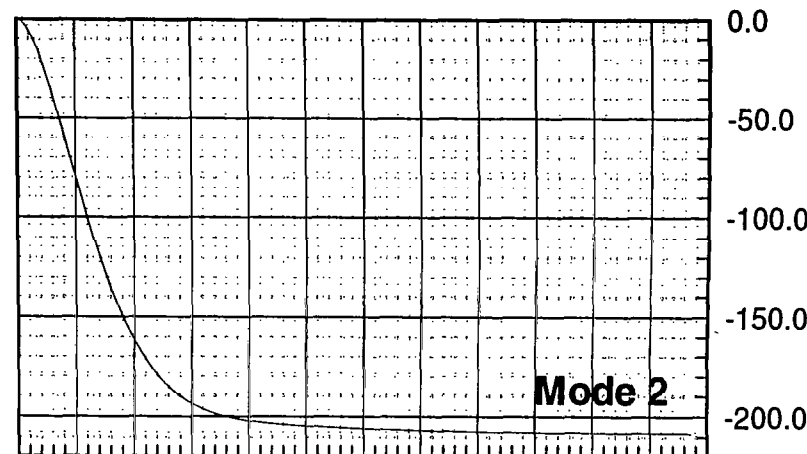
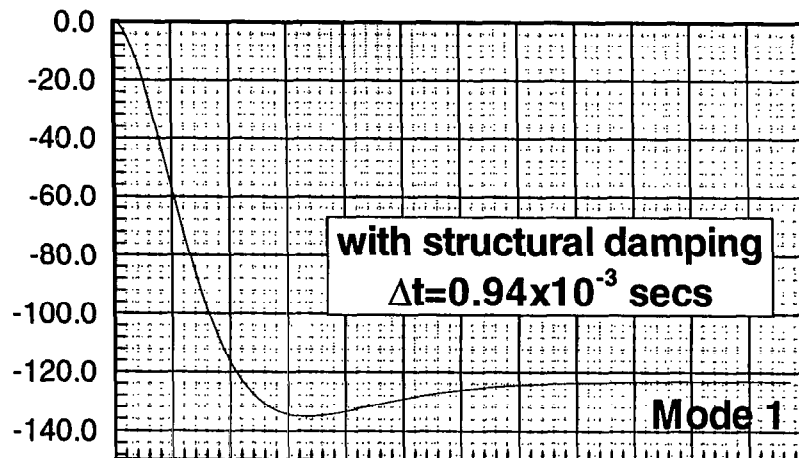
# Time History of Generalized Displacements for TCA W/B/LE Flap Aeroelastic Configuration, Static Case

High Speed Aerodynamics, Long Beach

CFL3D.AE-BA, N-S, Baldwin-Lomax (D-S),  $M_\infty=1.2$ ,  $\alpha=12.11^\circ$ ,  $q=758.3$  psf,  
( 93x281x69 C-O Grid )

Generalized  
Displacement

Generalized  
Displacement





# Flow Analysis of the TCA Wing/Body/LE Flap

The chart below shows a comparison of the flowfields for both rigid and aeroelastic configurations at  $\alpha = 12.11^\circ$  for the TCA wing/body with the outboard leading-edge flap deflected by  $8^\circ$ . The right wing of each configuration shows normalized cross-sectional total pressure cuts. The left wing shows surface  $C_p$  distributions and streamlines. Both configurations show strong leading-edge vortices. The shadow of the apex vortex is observed on the wing upper surface  $C_p$ 's (region of strong suction). As seen from the cross sectional pressure cuts, a secondary vortex is formed for both configurations. For this highly loaded case, the aeroelastic deflections are very obvious. The forebody vortex does not seem to affect the wing flowfield and seems to dissipate downstream of the trailing edge. The outboard leading-edge break vortex seems to be weaker for the aeroelastic configuration.



# Flow Analysis of the TCA Wing/Body/LE Flap



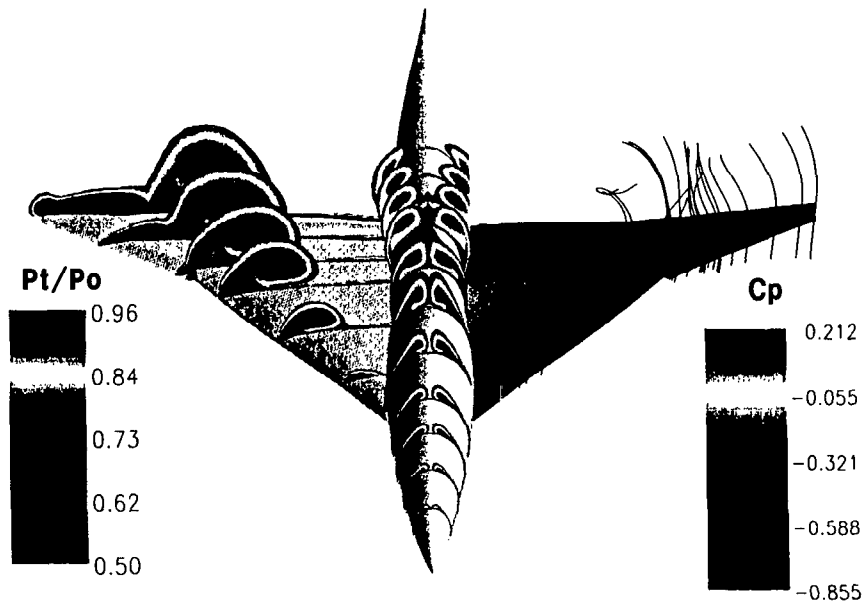
High Speed Aerodynamics, Long Beach

Configuration with and without Aeroelastic Deflections

Cross-Sectional Total Pressure Cuts, Surface  $C_p$  Distributions and Streamlines

CFL3D, N-S, Baldwin-Lomax D-S,  $M_\infty = 1.2$ ,  $\alpha = 12.11^\circ$ ,  $Re_c = 40$  million

(C-O Grid 93x281x69)



Rigid Configuration



Aeroelastic Configuration



# Pressure Distributions for TCA W/B/LE Flap

The figure below show the pressure cuts for the two solutions shown in the previous figure. The upper surface wing-apex vortex and the associated suction peaks are not significantly changed. When considering the airfoil cuts, at the 19.9% station the wing seems to be deflecting/twisting down, especially near the inboard nacelle. It was observed that the fuselage nose and aft-body sections were deflecting down, especially the aft-body section which seems to be more flexible. Consequently, the chordwise section of the 19.9% station that is coincident with the wing trailing-edge will be deflecting down.



# Pressure Distributions for the TCA W/B/LE Flap Rigid vs. Aeroelastic Configuration, Static Case



High Speed Aerodynamics, Long Beach

CFL3D.AE-BA, N-S, Baldwin-Lomax (D-S),  $M_\infty = 1.2$ ,  $\alpha = 12.11^\circ$ ,  $Re_c = 40$  million,  $q_\infty = 758.3$  psf

Span Station

85.0 %

68.0 %

53.9 %

41.3 %

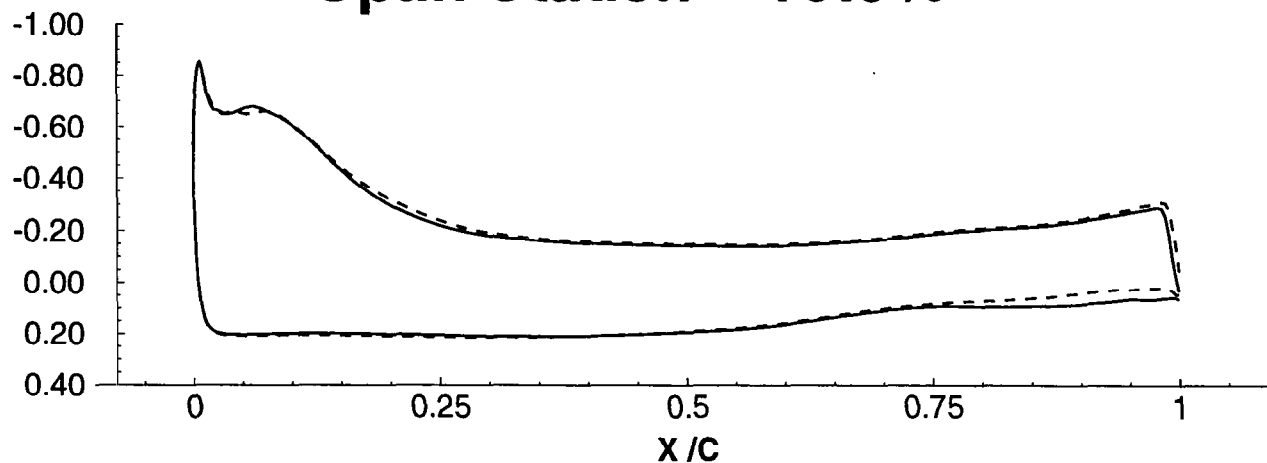
32.6 %

19.9 %

— Rigid  
- - Aeroelastic

$C_p$

Span Station = 19.9%



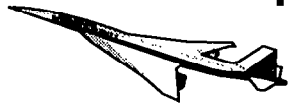
 **BOEING**

# Pressure Distributions for TCA W/B/LE Flap

Nevertheless, as one goes outboard, the deflections increase which is a usual aeroelastic trend for positive lift and the trailing edge deflects up as shown in the chart below.



# Pressure Distributions for the TCA W/B/LE Flap Rigid vs. Aeroelastic Configuration, Static Case



High Speed Aerodynamics, Long Beach

CFL3D.AE-BA, N-S, Baldwin-Lomax (D-S),  $M_\infty = 1.2$ ,  $\alpha = 12.11^\circ$ ,  $Re_c = 40$  million,  $q_\infty = 758.3$  psf

Span Station

85.0 %

68.0 %

53.9 %

41.3 %

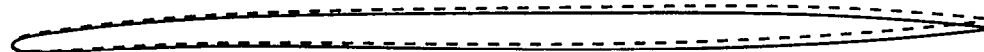
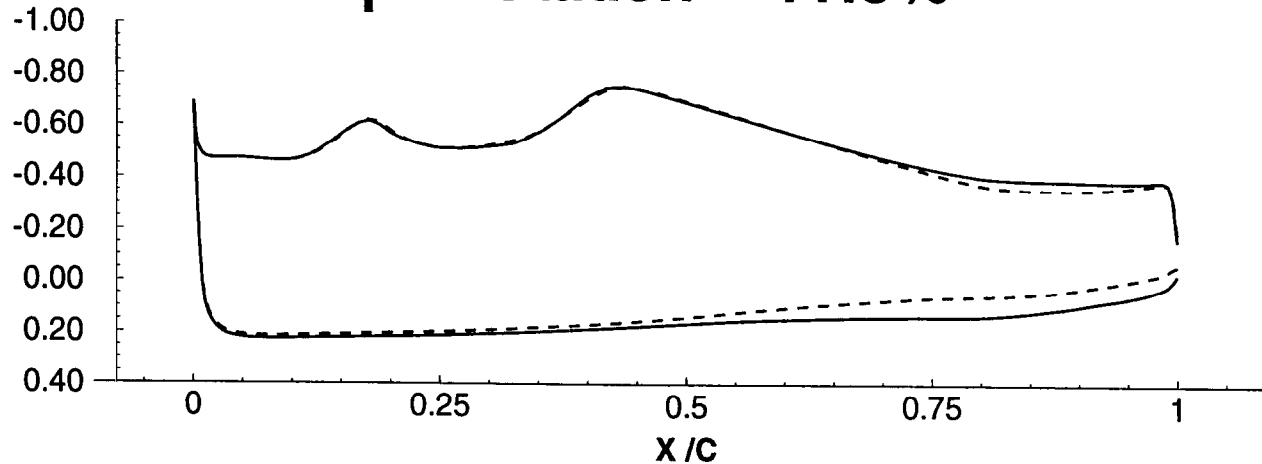
32.6 %

19.9 %

— Rigid  
- - Aeroelastic

$C_p$

Span Station = 41.3%



 **BOEING**

# Pressure Distributions for TCA W/B/LE Flap

The chart below shows a reduction in local incidence due to the structurally induced nose-down twist. The corresponding pressure distributions show a clear unloading of the 53.9% section.

UNITED ENGINEERING SYSTEMS  
[REDACTED]

# Pressure Distributions for the TCA W/B/LE Flap Rigid vs. Aeroelastic Configuration, Static Case



High Speed Aerodynamics, Long Beach

CFL3D.AE-BA, N-S, Baldwin-Lomax (D-S),  $M_\infty = 1.2$ ,  $\alpha = 12.11^\circ$ ,  $Re_c = 40$  million,  $q_\infty = 758.3$  psf

Span Station

85.0 %

68.0 %

53.9 %

41.3 %

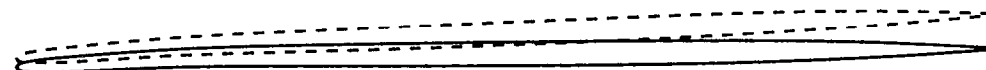
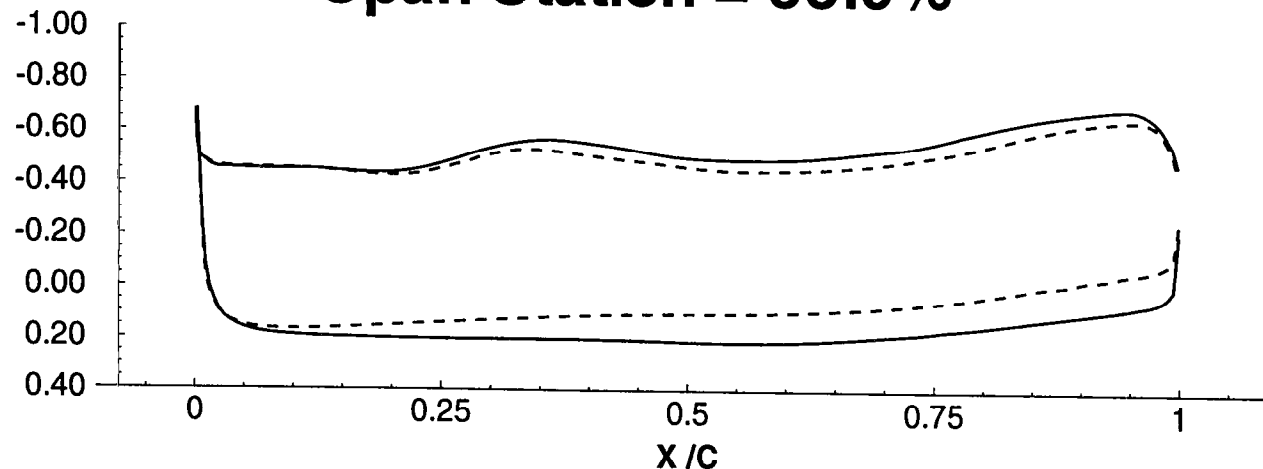
32.6 %

19.9 %

— Rigid  
- - Aeroelastic

$C_p$

Span Station = 53.9%



**BOEING**



# Pressure Distributions for TCA W/B/LE Flap

The same comments as in the previous chart apply here. When looking at the pressure curves, the leading-edge peak “squiggle” which is associated with the break vortex for the rigid configuration is absent for the aeroelastic configuration. This observation, agrees with the “weaker” leading-edge break vortex associated with the aeroelastic configuration observed in the flow analysis. Also, the trailing-edge shock seems to move aft with the aeroelastic deflections.



# Pressure Distributions for the TCA W/B/LE Flap Rigid vs. Aeroelastic Configuration, Static Case



High Speed Aerodynamics, Long Beach

CFL3D.AE-BA, N-S, Baldwin-Lomax (D-S),  $M_\infty = 1.2$ ,  $\alpha = 12.11^\circ$ ,  $Re_c = 40$  million,  $q_\infty = 758.3$  psf

Span Station

85.0 %

68.0 %

53.9 %

41.3 %

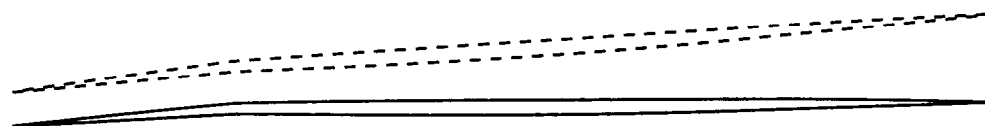
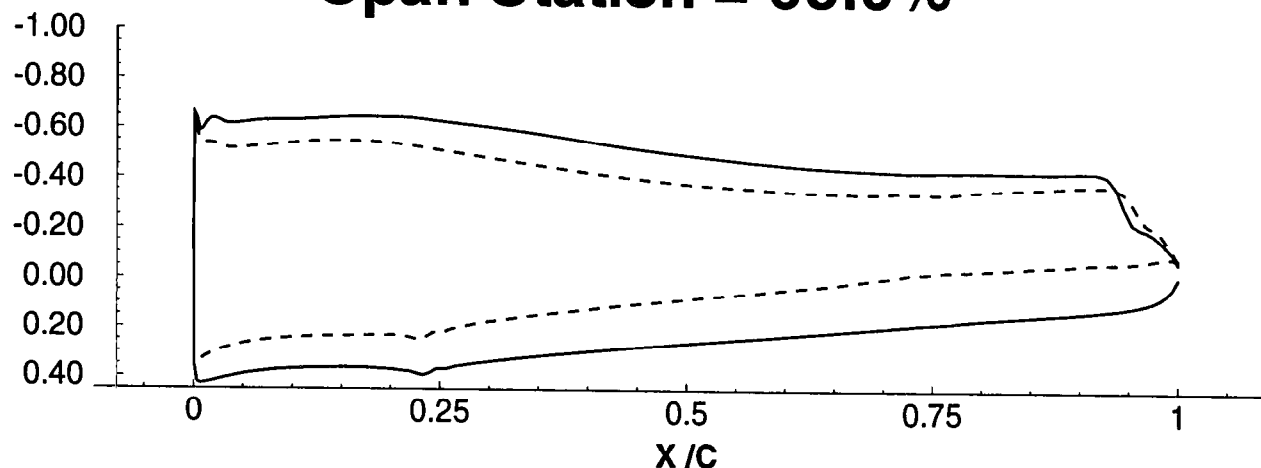
32.6 %

19.9 %

— Rigid  
- - Aeroelastic

$C_p$

Span Station = 68.0%



Contract No. NAS1-20220

**BOEING**

# Pressure Distributions for TCA W/B/LE Flap

The outboard sectional continue to show an unloading of the wing as the area defined by the  $C_p$  curves becomes smaller. Unlike the low angle-of-attack charts, the deflections near the tip are very large. For the 85% span station cut shown below the leading-edge pressure peak associated with the aeroelastic configuration tends to be more pronounced than the one for the rigid configuration.



# Pressure Distributions for the TCA W/B/LE Flap Rigid vs. Aeroelastic Configuration, Static Case



High Speed Aerodynamics, Long Beach

CFL3D.AE-BA, N-S, Baldwin-Lomax (D-S),  $M_\infty = 1.2$ ,  $\alpha = 12.11^\circ$ ,  $Re_c = 40$  million,  $q_\infty = 758.3$  psf

Span Station

85.0 %

68.0 %

53.9 %

41.3 %

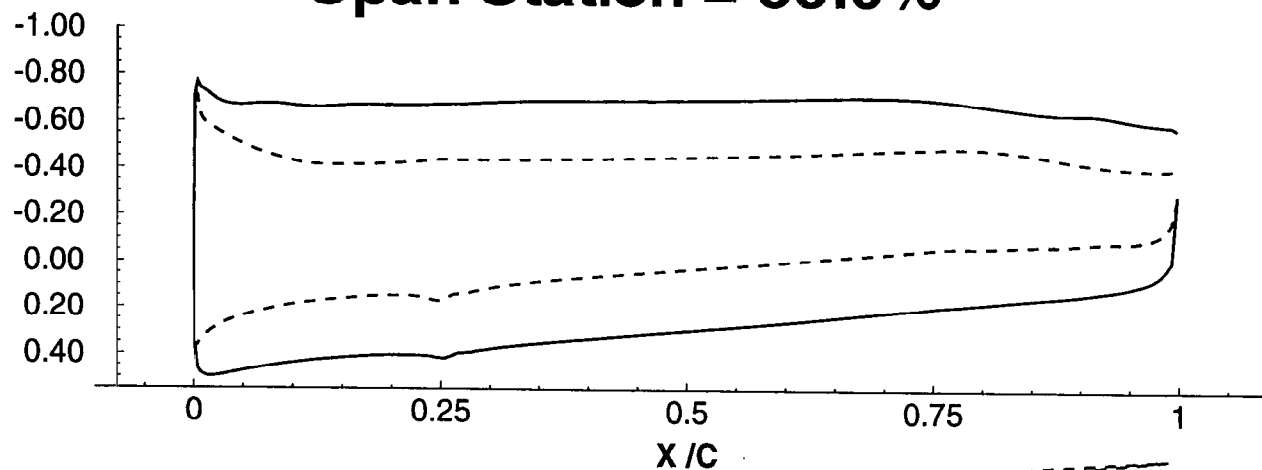
32.6 %

19.9 %

— Rigid  
- - Aeroelastic

$C_p$

Span Station = 85.0%



# Time History of the Generalized Displacements for the TCA W/B/LE Flap, Flutter Case

The figure below shows the time histories of the same for generalized deflections plotted for the flutter run at  $\alpha = 2.83^\circ$ . The time step used is the same as that of the static case. The three first modes seem to be in phase, with mode 1 increasing in oscillation amplitude. Mode 7 shows the interaction of several frequency components.



# Time History of Generalized Displacements for TCA W/B/LE Flap Aeroelastic Configuration, Flutter Case

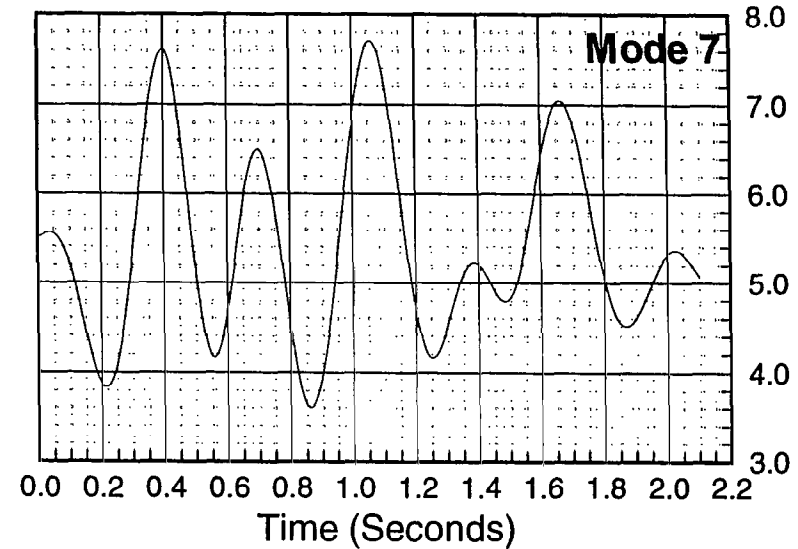
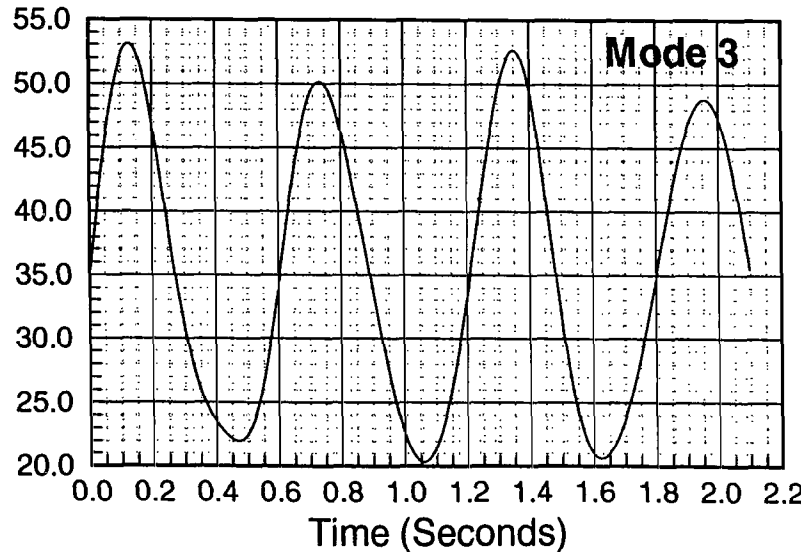
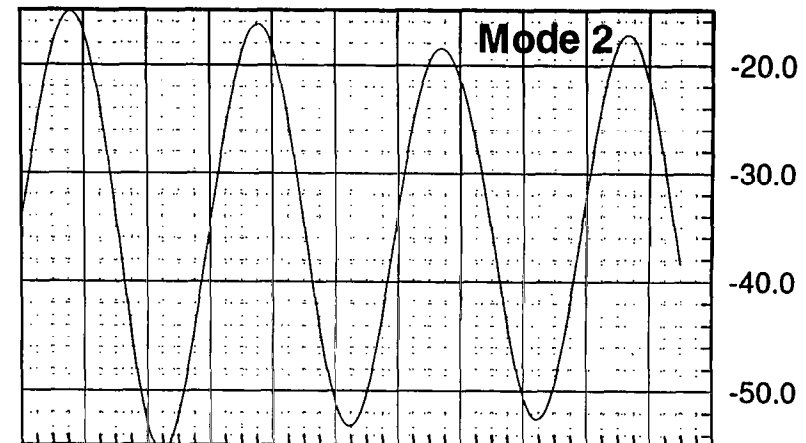
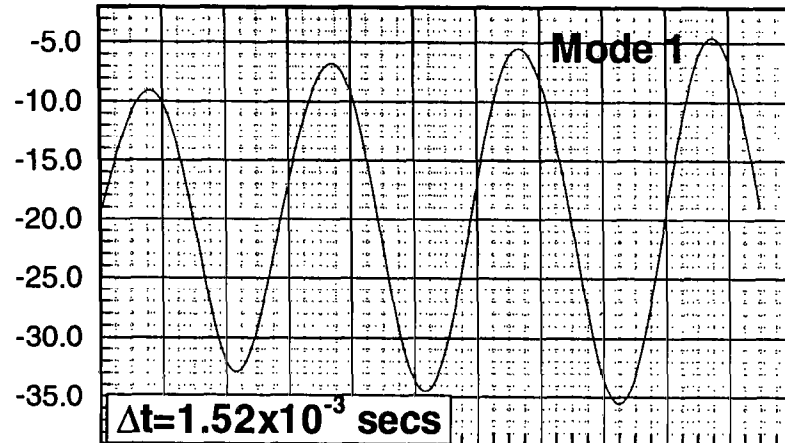


High Speed Aerodynamics, Long Beach

CFL3D.AE-BA, N-S, Badwin-Lomax (D-S),  $M_\infty=1.2$ ,  $\alpha=2.83^\circ$ ,  $q_\infty=758.3$  psf  
(93x281x69 C-O Grid)

Generalized  
Displacement

Generalized  
Displacement



██████████ E ██████████ 20.



# Pressure Distributions for the TCA W/B/LE Flap Aeroelastic Configuration, Flutter Case

The figure below shows six pressure cuts at 4 different points in time of the last period of the generalized displacements corresponding to mode 1. The overall variation in pressures from peak to trough seems minimal. However, from 41.3% to 53.9% stations, where the engine influence seems to be the greatest, the differences in pressure seem to be most significant. It is worthwhile to note that the pressures at  $T/4$  and  $3T/4$  match exactly, which suggests a very “quasi-steady” state of the aerodynamics, in which the aerodynamic loads are mostly dominated by their steady components (usually the case with small frequency oscillations). This is coincident with the large outboard engine pitching component included in the dominant vibration modes.



# Time History of the Generalized Displacements for the TCA W/B/LE Flap, Flutter Case

The figure below shows the time histories of the same generalized deflections plotted for the flutter run at  $\alpha = 12.11^\circ$ . The time step used is the same as that of the static case. The first three modes seem to be in phase in this case as well with mode 7 showing interaction of several frequency components. Note that the amplitude of mode 1 does not appear to be increasing.





# Time History of Generalized Displacements for TCA W/B/LE Flap Aeroelastic Configuration, Flutter Case

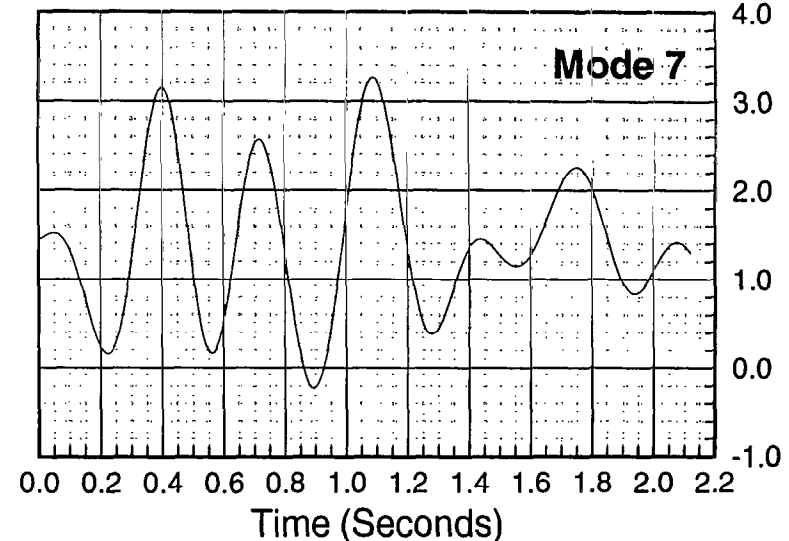
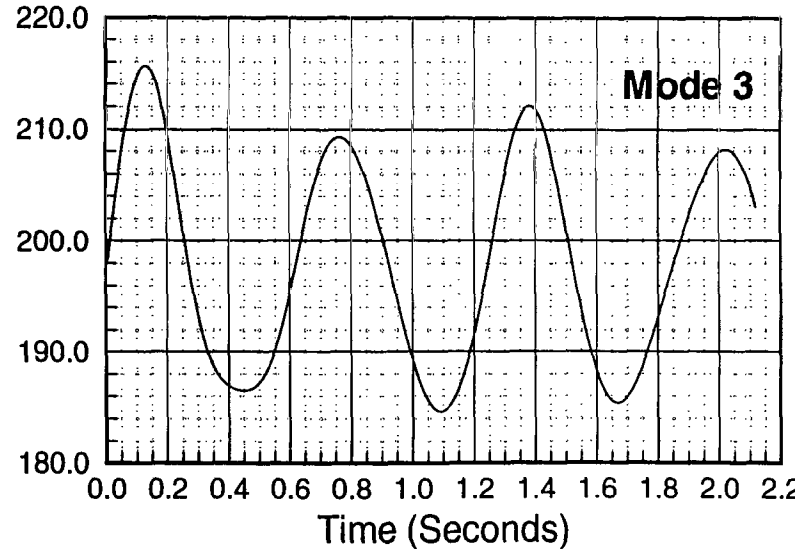
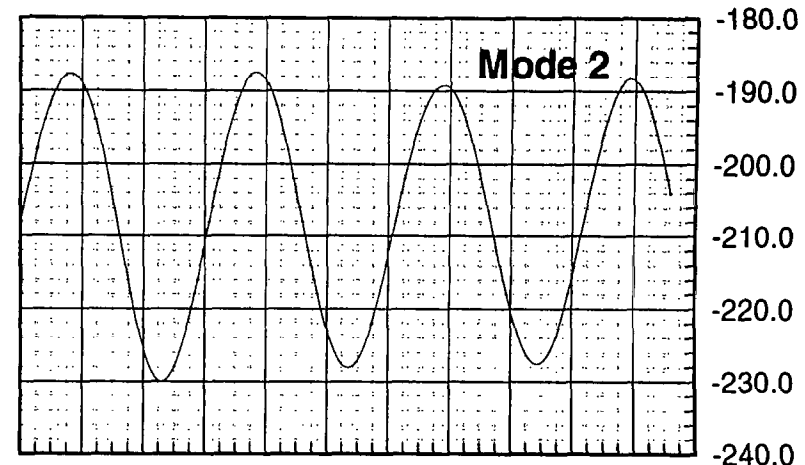
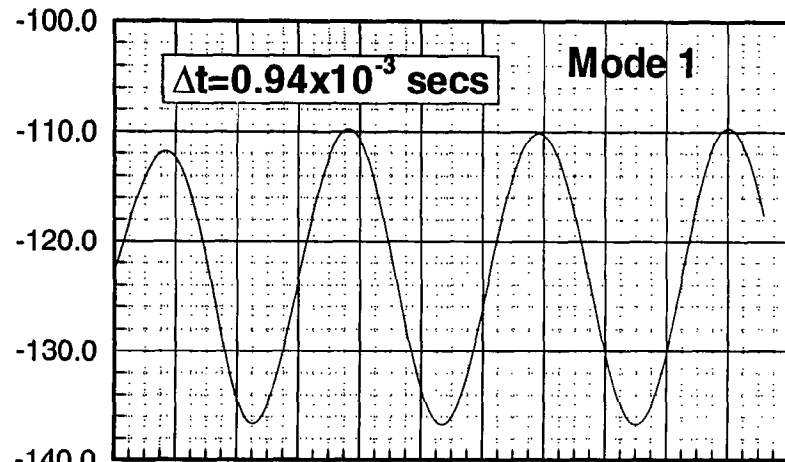


High Speed Aerodynamics, Long Beach

CFL3D.AE-BA, N-S, Baldwin-Lomax (D-S),  $M_\infty=1.2$ ,  $\alpha=12.11^\circ$ ,  $q_\infty=758.3$  psf  
(93x281x69 C-O Grid)

Generalized  
Displacement

Generalized  
Displacement



# Pressure Distributions for the TCA W/B/LE Flap Aeroelastic Configuration, Flutter Case

The figure below shows six pressure cuts at 4 different points in time of the last period of the generalized displacements corresponding to mode 1 at  $\alpha = 12.11^\circ$ . The overall variation in pressures from peak to trough is again small. Again, from 41.3% to 53.9% stations, where the engine influence seems to be the greatest, the differences in pressure seem to be most significant. However, the relative change in pressures between peaks and troughs is smaller than the small angle-of-attack case. It is worthwhile to note that the suction peaks due to the wing-apex vortex remain unchanged.

■



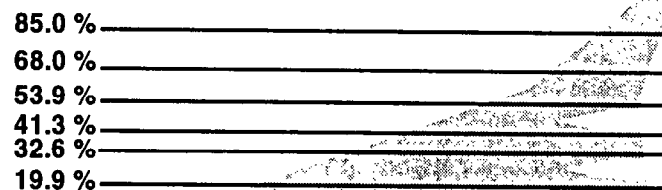
# Pressure Distributions for the TCA W/B/LE Flap Aeroelastic Configuration, Flutter Run, Last Period of Mode1 Gen. Displ.



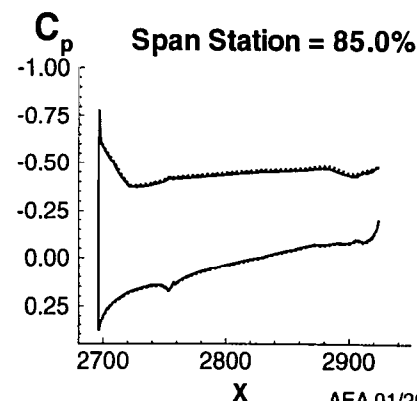
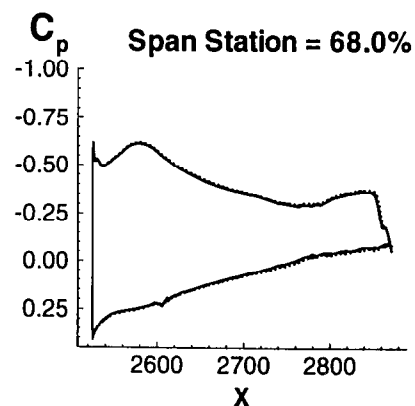
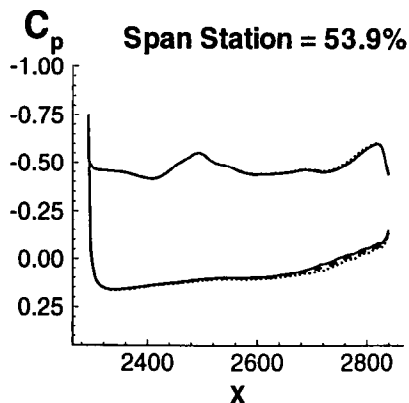
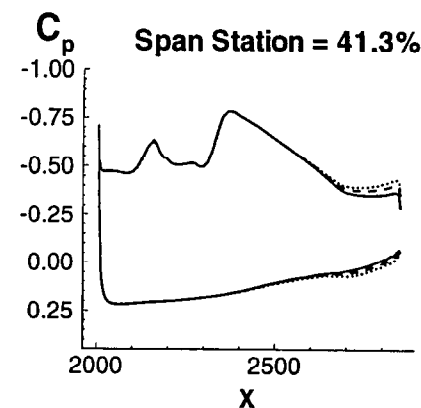
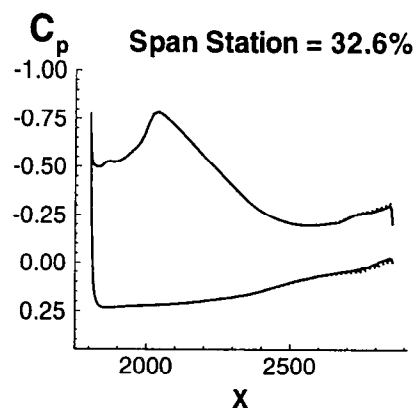
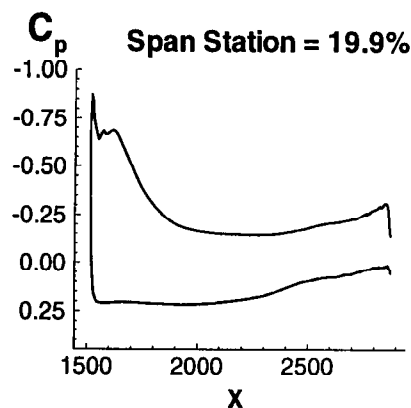
High Speed Aerodynamics, Long Beach

CFL3D.AE-BA, N-S, Baldwin-Lomax (D-S),  $M_\infty = 1.2$ ,  $\alpha = 12.11^\circ$ ,  $Re_c = 40$  million,  $q_\infty = 758.3$  psf

Span Station



— Trough  
- - - T/4  
... Peak  
— 3T/4

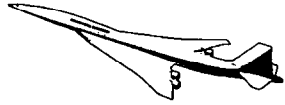


AEA 01/29/98

# System ID Results

The table below shows a comparison of the eigenvalues from system ID analyses for each of the CFL3D runs with the linear theory results. Note that the system ID algorithm did not produce an eigenvalue corresponding to modes #5 and #10 on the linear analysis. This is not surprising, since these are near-repeat roots, and would be difficult to identify with any algorithm. The frequency and damping results are discussed separately on the subsequent slides.





# System ID Results

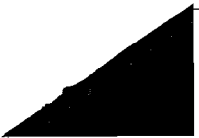
High Speed Aerodynamics, Long Beach

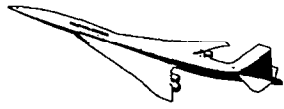
- Comparison of Eigenvalues from System ID
- “Near Repeated” Roots Not Captured
- Minor Damping Variations, But No Dramatic Instabilities

Mode	Linear		CFL3D, 3 degrees		CFL3D, 12 degrees	
	Frequency	Damping	Frequency	Damping	Frequency	Damping
1	1.44	-.0173	1.44	-.0272	1.41	-.0436
2	1.67	-.0196	1.69	-.0074	1.65	-.0128
3	2.01	-.0105	1.99	-.0154	1.99	-.0124
4	2.52	-.0693	2.47	-.0396	2.46	-.0688
5	2.68	-.0094				
6	2.69	-.0045	2.72	-.0166	2.71	-.0134
7	3.21	-.0921	3.16	-.0552	3.03	-.0994
8	4.05	-.0650	4.06	-.0304	4.05	-.0868
9	4.25	-.0683	4.24	-.0584	4.17	-.0364
10	4.91	-.0310				
11	5.00	-.0032	5.00	.0128	5.01	-.0130
12	5.25	-.0164	5.19	-.1312	5.24	-.0162

# System ID Results - (Cont'd)

As seen in the bar chart below, the frequencies obtained from System ID results for the two angle-of-attack conditions correlate very well with each other and with linear analysis. As mentioned above, mode 5 and mode 10 are not identified by the system ID algorithm.



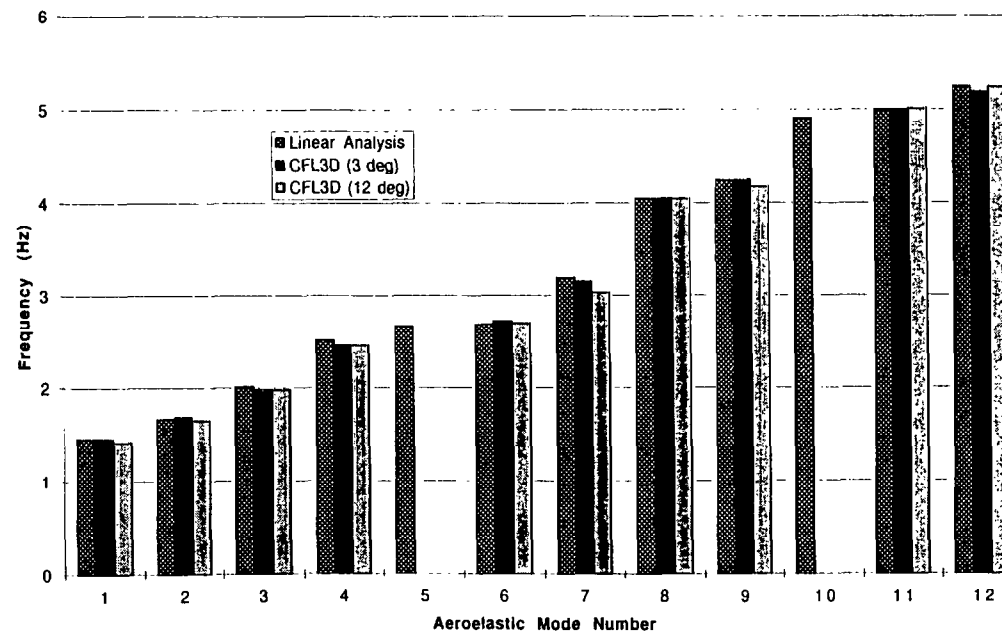


# System ID Results

High Speed Aerodynamics, Long Beach

- Frequencies Correlate Very Well With Linear Analysis
- Near-Repeat Roots Missed

Comparison of Aeroelastic Frequencies



# System ID Results - (Cont'd)

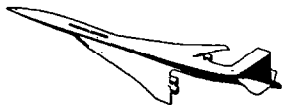
This chart compares modal damping estimates from the low- $\alpha$  and high- $\alpha$  CFL3D solutions with linear predictions. Aeroelastic damping is much more sensitive to aerodynamics than frequency, so more significant variations are seen here.

For most modes, the high- $\alpha$  damping values are more negative (more stable) than the low- $\alpha$  results, and tend to correlate better with the linear theory results.

There is no evidence that the high- $\alpha$  aerodynamics have a strong destabilizing effect for this flight condition.





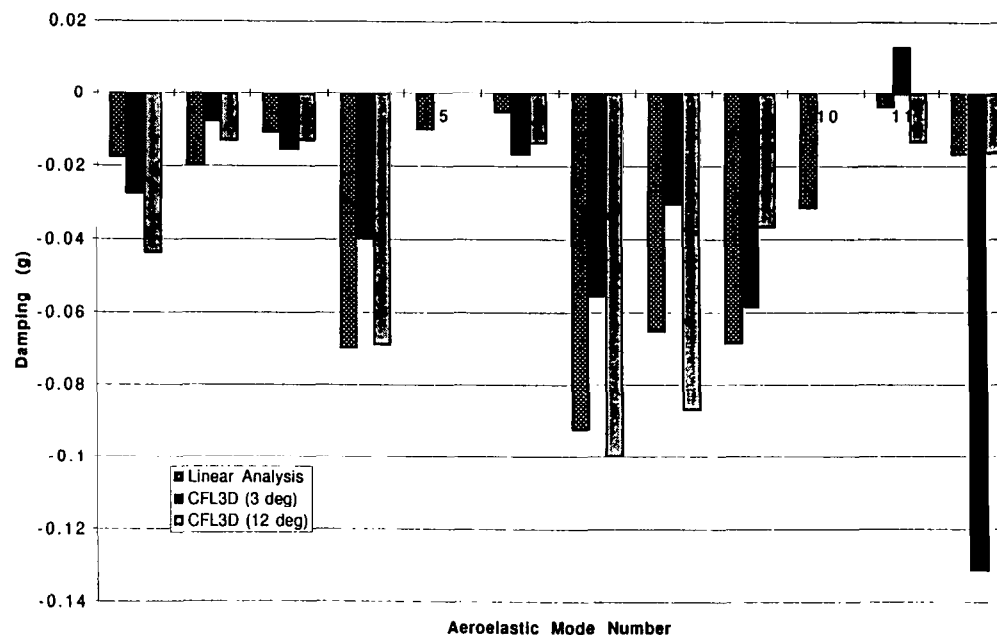


# System ID Results

High Speed Aerodynamics, Long Beach

- Damping Results Correlate Marginally With Linear Analysis
- No Indication that High- $\alpha$  Aero Induces Instability

Comparison of Aeroelastic Damping

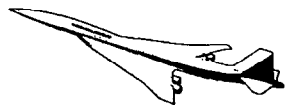


## System ID Results - (Cont'd)

While the SYSID code can be used to generate Q-G and Q-F plots from time domain flutter results, this was not possible due to the missing roots discussed earlier.

Modifications to the SYSID algorithm to avoid this problem are currently being investigated.





# System ID Results

High Speed Aerodynamics, Long Beach

- Q-G and Q-F Plots Could Not Be Constructed
- Formulation Requires All Eigenvalues to Be Identified
- Missed Roots or Spurious Roots Corrupt Interpolation
- Possible Enhancements:
  - Deflation
  - RLS Formulation

# Conclusions

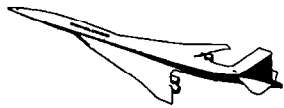
The CFL3D aeroelastic frequencies seem to correlate fairly well with linear analyses, while damping results vary significantly (especially for the low  $\alpha$  case). The high angle-of-attack case does not show evidence of any new instabilities.

It is possible that a leading-edge vortex induced instability might exist at other flight conditions, particularly at an intermediate angle-of-attack where the leading-edge vortex begins to form.

An experimental evaluation of high- $\alpha$  effects on flutter is planned for the Aeroelastic Semispan Model (ASM) test in 1999.



# Conclusions



High Speed Aerodynamics, Long Beach

- CFL3D Aeroelastic Frequencies Correlate Fairly Well With Linear Analysis.
- CFL3D Damping Results Vary Significantly.
- No Evidence of New Instability at 12 degrees AOA.
- Could Investigate Intermediate Angles When LE Vortex Begins Forming.
- Other Mass Conditions, Mach Numbers?

